Mossbauer study of magnetic interactions in nanocrystalline $Fe_{73.5}Cu_1Nb_3Si_{16.5}B_6$

1995 J. Phys.: Condens. Matter 7 2237

(http://iopscience.iop.org/0953-8984/7/10/029)

J. Phys.: Condens. Matter 7 (1995) 2237–2248. Printed in the UK

Mössbauer study of magnetic interactions in nanocrystalline $Fe_{73.5}Cu_1Nb_3Si_{16.5}B_6$

Ajay Gupta†, Neeru Bhagat† and G Principi‡

† School of Physics, Devi Ahilya University, Indore 452001, India
‡ Dipartimento di Ingegneria Meccanica, Sezione Materiali, Universita di Padova, Via Marzolo 9, 35131 Padova, Italy

Received 8 July 1994, in final form 15 November 1994

Abstract. Mössbauer spectroscopy has been used to follow the temperature-dependent magnetization in the temperature range 4.2–823 K of the amorphous as well as the nanocrystalline grains in partially crystallized $Fe_{73.5}Cu_1Nb_3Si_{16.5}B_6$ alloy. In nanocrystallized specimens, the magnetization behaviour of both amorphous and nanocrystalline components is significantly different from that of the bulk amorphous or crystalline Fe_3Si. Initially the nanocrystalline grains exhibit a superparamagnetic behaviour above the Curie temperature of the amorphous matrix. With increasing density of nanocrystalline grains, the superferromagnetic interaction between the grains becomes important.

1. Introduction

Fe-based nanocrystalline alloys obtained by controlled partial crystallization of some Fe–Cu–Nb–Si–B amorphous alloys are being studied extensively because of their excellent soft magnetic properties. These alloys exhibit a large saturation magnetization together with very low magnetostriction (about 10^{-6}) [1]. Structural studies have shown that the nanocrystalline phase consists of non-stoichiometric BCC Fe_3Si particles of approximate size 10 nm embedded in an amorphous matrix [1–3]. Both the nanocrystalline and the amorphous grain boundary phases are ferromagnetic at room temperature and the excellent soft magnetic properties of this composite system occur as a result of the averaging over the two phases [4, 5]. In order to understand the excellent soft magnetic properties of nanocrystalline alloys, it is important to understand the magnetic behaviour of both the amorphous matrix and the nanocrystalline grains and the interaction between the two.

Because of the small crystallite size the nanocrystalline particles qualify as single-domain particles and may exhibit interesting magnetic properties associated with single-domain particles [6]. Indirect experimental evidence for superparamagnetism in nanocrystalline grains has been provided by Slawaska-Wainewska *et al* [7], through field-dependent magnetization measurements at elevated temperatures. Mössbauer spectroscopy is a unique technique which can follow the magnetization behaviour of both amorphous and nanocrystalline phases separately. Therefore, in the present work we have used Mössbauer spectroscopy in order to study the magnetization behaviour of the nanocrystalline grains as well as the amorphous grain boundary phase, and also to obtain information about the magnetic interaction between the amorphous matrix and the nanocrystals.

0953-8984/95/102237+12$19.50

2. Experimental details

Amorphous alloy ribbons, prepared by the melt-spinning technique, having the composition $Fe_{73.5}Cu_1Nb_3Si_{16.5}B_6$, were obtained from Vacuumschmeltz GmbH, Hanau. Thermal treatments were performed in a vacuum of 10^{-5} mbar. An evacuated quartz tube containing the samples was dipped in a pre-heated salt bath for the isothermal treatments at 813 K for different periods of time in order to induce different degrees of crystallization. The various annealing times were 0 min (specimen A0), 2 min (specimen A2), 10 min (specimen A10) and 25 min (specimen A25).

Mössbauer spectra of the samples were taken using a ^{57}Co:Rh source. Temperature-dependent Mössbauer studies of these samples were carried out in the range 4.2–823 K. X-ray diffraction studies were made with a Siemens D5000 diffractometer using Cu Kα radiation.

3. Results and discussion

Figure 1 gives some of the representative temperature-dependent Mössbauer spectra of the specimens in an as-received state and after annealing at 813 K for different periods of time. The spectrum of the as-received specimen consists of a broad sextet characteristic of the amorphous state. In the spectra for specimens A10 and A25, several additional sharp lines indicate the presence of the crystalline phase. In specimen A2, because of the small amount of crystallization, the peaks due to crystalline phase can be seen only as small humps (figure 1(*b*)). Additional evidence for the existence of nanocrystalline phase in this specimen is provided from the XRD data.

The Mössbauer spectra of specimens A0 and A2 were analysed with a distribution of hyperfine fields, while those of specimens A10 and A25 were analysed using the superposition of one amorphous component and four crystalline sextets corresponding to different iron sites in the non-stoichiometric Fe_3Si compound [3, 8, 9]:

(i) iron atoms at site D;
(ii) iron atoms at site A with four Fe near neighbours (A_4);
(iii) iron atoms at site A with three Si near neighbours (A_5);
(iv) iron atoms at site A with two Si near neighbours (A_6).

The lineshape of the amorphous component was taken to be a Voigt profile, in order to account for the distribution of the hyperfine fields. The lineshape of crystalline components was taken to be Lorentzian. The computer fits to the experimental data are shown by the solid curves in figure 1. Details of the fitting for some representative spectra of specimen A25 at 300 and 723 K are shown in figure 2 where all the subspectra corresponding to the crystalline as well as the amorphous components are plotted separately. The hyperfine parameters of different subcomponents of the room-temperature Mössbauer spectra of the specimens are given in table 1. The hyperfine parameters of the four crystalline subspectra in specimens A10 and A25 compare well with those of the non-stoichiometric Fe_3Si [9]. The Mössbauer spectra at temperatures other than room temperature were fitted by constraining the relative areas of different crystalline components to the values obtained from the fittings of the room-temperature spectra. The area ratio of the amorphous to crystalline components was taken as a free parameter, in order to take into account different recoilless fractions of amorphous and crystalline components. The relative areas of various crystalline components obtained from the fitting of the room-temperature data were used to obtain the composition

of the crystalline phase [3]. The amount of the amorphous phase in a partially crystallized specimen was determined from its percentage area at 4.2 K.

Figure 3 gives the x-ray diffractograms of the four specimens in the 2θ range 35–55°. The average crystallite size was determined from the line profile analysis of the [110] reflection of the nanocrystalline phase using the Scherrer method. The crystalline peak was separated from the amorphous background by subtracting the XRD pattern of the specimen A0 from that of the partially crystallized specimen after appropriate normalization. The crystalline peak was least squares fitted with a pseudo-Voigt profile (figure 4) in order to obtain accurate linewidths. The correction for the instrumental broadening was done by subtracting the width of the [110] reflection of a well annealed foil of α-iron from that of the nanocrystalline phase. Table 2 gives the fraction of the crystallized component as obtained from the Mössbauer spectra and the crystallite size determined from XRD for different specimens.

3.1. Magnetization behaviour of amorphous components

Figure 5 gives the temperature-dependent hyperfine field of specimen A0. The solid curve represents the fit of the data with the theory of Handrich [10]. It was found necessary to take a temperature-dependent exchange fluctuation parameter δ of the form [11, 12]

$$\delta(T) = \delta_0(1 - \alpha T^2) \tag{1}$$

in order to achieve reasonably good fitting of the experimental data. It has been shown by Kaneyoshi *et al* [12] that a distribution of magnetic moments, in addition to that of the exchange interactions, leads to a temperature-dependent δ. A significantly large value of α in the present specimen indicates a relatively large distribution of magnetic moments. This large distribution of Fe magnetic moments may be attributed to the presence of Cu and Nb atoms which are known to reduce the magnetic moment of their Fe near neighbours [13].

Table 1. The hyperfine fields and relative areas of different subcomponents of room-temperature Mössbauer spectra of partially crystallized $Fe_{73.5}Cu_1Nb_3Si_{16.5}B_6$ specimens. For comparison, the parameters of non-stoichiometric Fe_3Si (18.4% Si), as taken from [9], are also included.

		Fitted parameters				
			Crystalline sites			
Specimen		Amorphous component	D	A_4	A_5	A_6
A0	B_{hf}(T)	21.0				
	RA (%)	100				
A2	B_{hf}(T)	21.4	31.1	19.7		
	RA(%)	94	3	3		
A10	B_{hf}(T)	19.5	31.6	19.7	24.5	28.6
	RA(%)	54	15	17	11	3
A25	B_{hf}(T)	18.2	31.7	19.8	24.7	28.6
	RA(%)	44	17	20	14	5
$Fe_{0.816}Si_{0.184}$	B_{hf}(T)	18.2	32.3	19.4	24.5	28.9

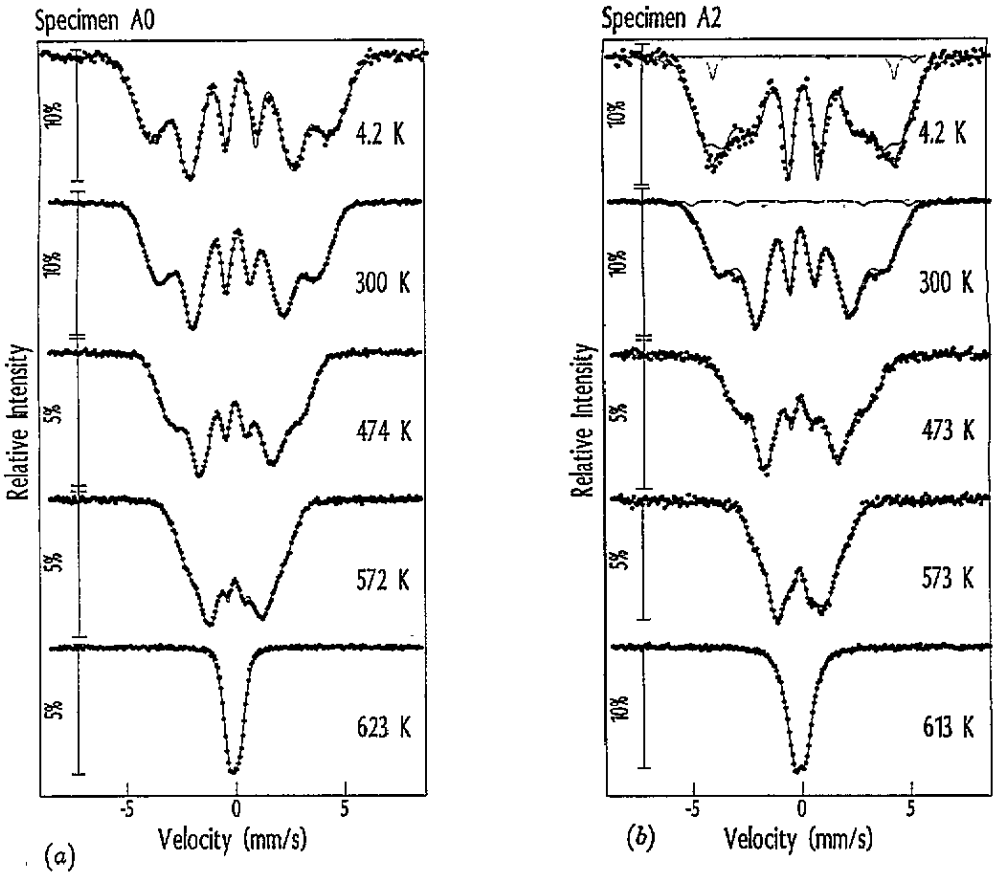

Figure 1. Temperature-dependent Mössbauer spectra of various specimens: (*a*) A0; (*b*) A2, (*c*) A10, (*d*) A25.

Figure 6 gives the reduced hyperfine field of the amorphous component in specimens A10 and A25 as a function of reduced temperature. It is evident that the temperature dependence of hyperfine fields for these specimens is markedly different from that for specimens A0 and A2. The solid curves are the fits obtained with the theory of Handrich. However, the fits are rather poor, especially in the low-temperature region. This unusual temperature dependence of the hyperfine field of amorphous components may partly be attributed to increased fluctuations in exchange interaction as well as the magnetic moment originating from increased compositional inhomogeneity in the amorphous phase, and partly to the magnetic interaction with the crystalline phase.

In the critical region, the temperature dependence of the hyperfine field may be written as

$$B_{hf}(T) = A(T_C - T)^{\beta} \tag{2}$$

T_C being the Curie temperature. In amorphous ferromagnets this behaviour is found to hold over a much larger temperature range extending well beyond the critical region [14] and Mössbauer measurements have been used to estimate the critical exponent β.

Figure 7 gives the fit of the high-temperature magnetization data of the specimens A0 and A25 with equation (2). It is evident that for specimen A0 the hyperfine field follows

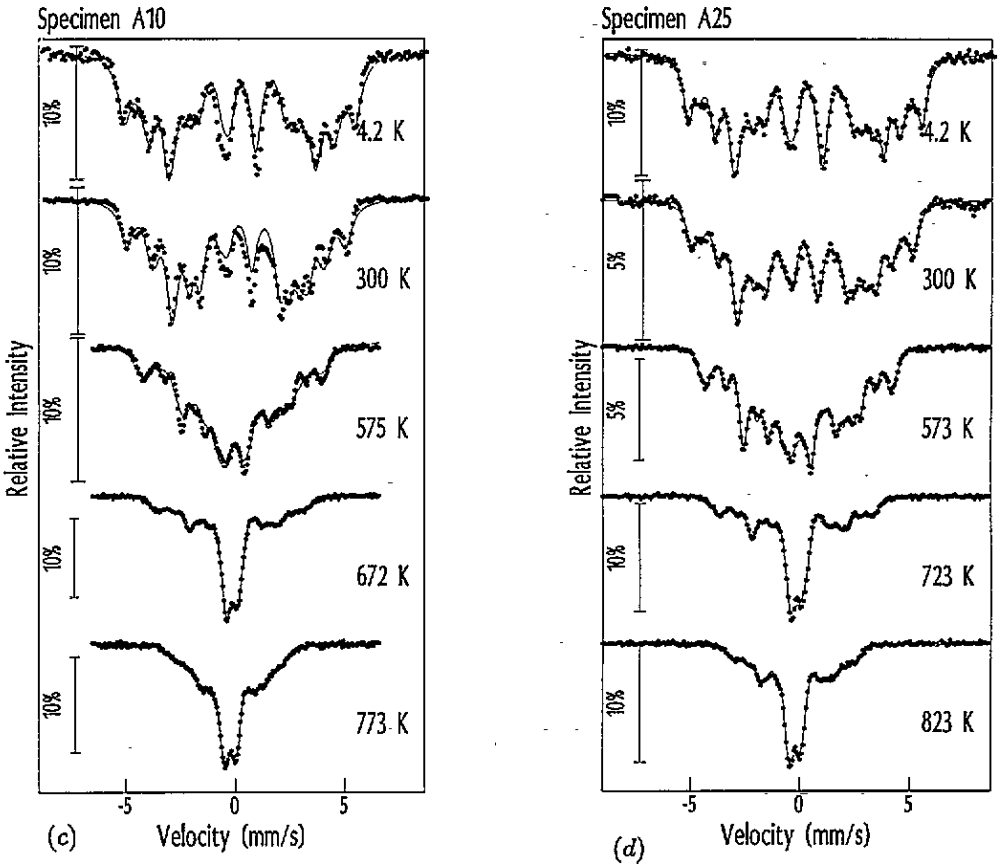

Figure 1. (Continued)

equation (2) down to about 425 K (i.e. $0.71T_C$), while for specimen A25 the above relation holds down to about 375 K (i.e. $0.65T_C$). Table 3 summarizes the results of the least-squares fitting of the high-temperature data, of all the four specimens, with equation (2). Perusal of table 3 shows that initially T_C exhibits a small increase upon annealing for 2 min, which may be attributed to the structural relaxation associated with annealing. For a longer annealing time a decrease in T_C with increasing crystallization is a consequence of the enrichment of the amorphous phase in boron. In the as-received specimen the value of the critical exponent β is close to the theoretical value for a three-dimensional Heisenberg ferromagnet [15]. With increasing crystallization the value of β decreases and for specimen A25 it attains a value in between that for three-dimensional and two-dimensional systems [15]. It may be noted that, as the amount of crystalline phase increases, the thickness of the amorphous grain boundary phase decrease; for a sufficiently thin grain boundary layer the dimensionality cannot be taken as 3, and low-dimensional magnetic behaviour should be observed. Here it should be noted that, although the spins in the grain boundary layer also interact with those in the crystallites, this interaction is much weaker than that between the spins within the grain boundary layer. This is supported by the fact that there exists a well defined T_C for the amorphous layer which is only slightly affected by increasing the amount of nanocrystalline phase (causing an increase in the interaction of the spins of

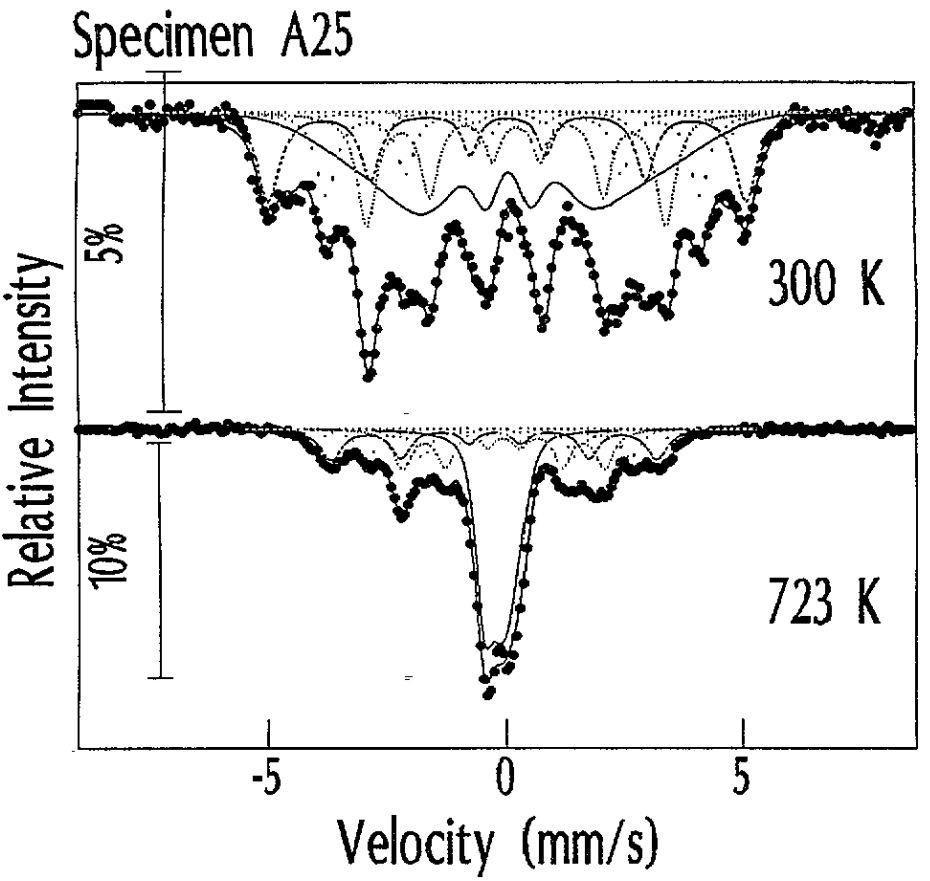

Figure 2. Details of the fitting of the Mössbauer spectra of specimen A25 at 300 and 723 K. The five subcomponents correspond to (*a*) Fe atoms in the amorphous phase, (*b*) Fe atoms on D sites, (*c*) Fe atoms on A_4 sites, (*d*) Fe atoms on A_5 sites and (*e*) Fe atoms on A_6 sites.

Table 2. Values of the crystalline component, crystallite size and lattice parameter for samples A2, A10 and A25.

Specimen	Fraction of crystallized component (%)	Crystallite size (nm)	Lattice parameter (Å)
A2	4.0	4.6	5.753
A10	33.7	10.4	5.665
A25	43.0	9.3	5.679

the amorphous layer with those in crystallites). Thus, the temperature dependence of the magnetization of the amorphous layer is mainly determined by the interaction between the spins within the amorphous layer.

On the assumption of a uniform thickness d for the amorphous grain boundary layer (figure 8), the total volume of the amorphous phase can be written as

$$V_a = sd/2 \tag{3}$$

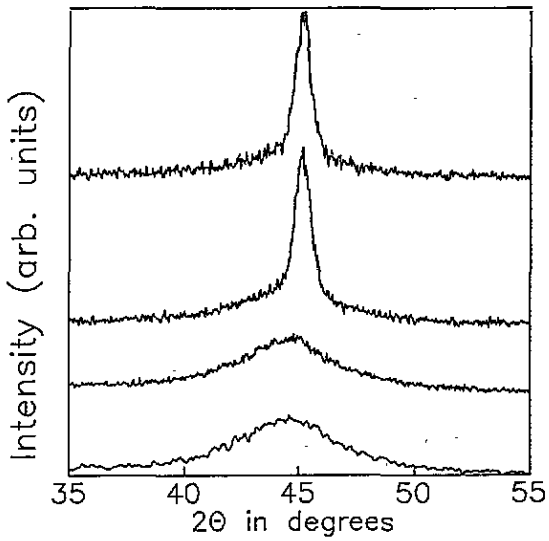

Figure 3. X-ray diffractograms of the four specimens in the range $35° < 2\theta < 55°$.

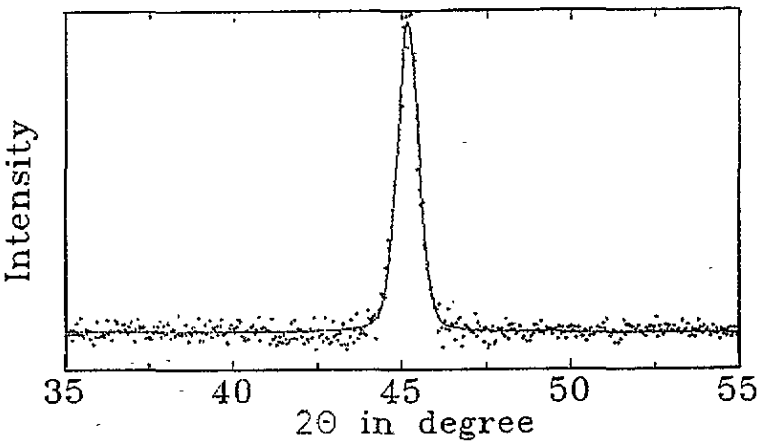

Figure 4. X-ray diffractogram of specimen A25 after subtracting the contribution due to amorphous component. The solid curve represents a least-squares fit of the data with a pseudo-Voigt profile.

Table 3. Results of the least-squares fitting of the high-temperature data for the four specimens A0, A2, A10 and A25.

Specimen	Temperature range (K)	A	T_C (K)	β
A0	424–596	2.86	600.5	0.35
A2	423–576	3.17	608.4	0.33
A10	372–526	2.90	567.6	0.33
A25	375–573	3.92	578.0	0.26

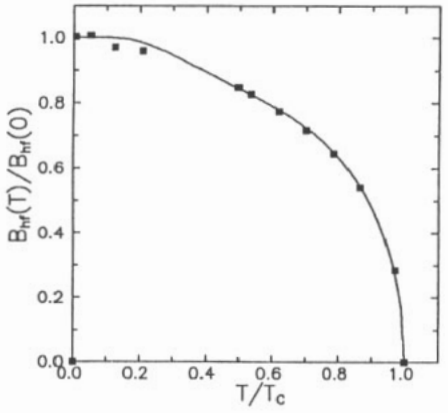

Figure 5. Temperature-dependent hyperfine field for specimen A0. The solid curve represents the fit of the data using the theory of Handrich with a temperature-dependent exchange fluctuation parameter δ.

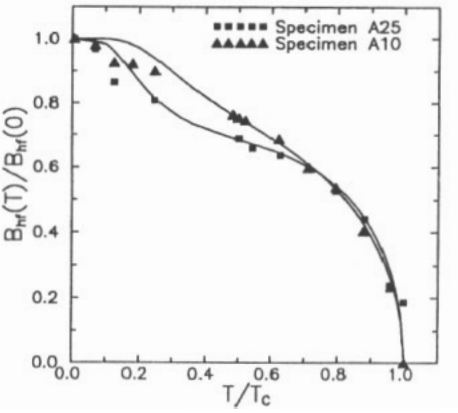

Figure 6. Reduced hyperfine field of the amorphous component for specimens A10 and A25. The solid curve represents the fit of the data using the theory of Handrich with a temperature-dependent exchange fluctuation parameter δ.

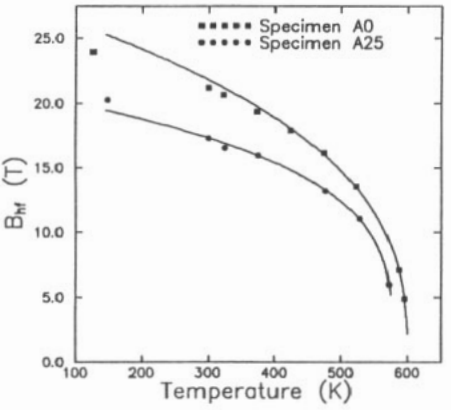

Figure 7. Fit of the high-temperature hyperfine field data of the amorphous component for specimens A0 and A25 with equation (2).

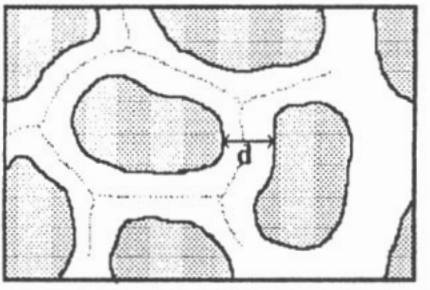

Figure 8. Schematic diagram of the microstructure of nanocrystallized specimen used for calculating the thickness of the grain boundary layer.

s being the total surface area of the nanocrystalline grains. Further, taking a spherical shape of the nanocrystals, the volume fraction occupied by the amorphous phase can be written as

$$f_a = \frac{V_a}{V_a + V_c} = \frac{3d}{3d + 2r} \tag{4}$$

r being the average radius of the nanocrystalline grains. If we neglect the difference between the densities of the two phases a rough estimate of the grain boundary layer thickness is

$$d = \frac{2r}{3}\frac{f_a}{f_c} \tag{5}$$

where f_a and f_c are the fractional amounts of amorphous and crystalline phases, respectively. Using the data in table 2 the thickness of the grain boundary layer for specimen A25 is

estimated to be about 42 Å. This is an upper estimate since any shape of the crystallites other than spherical would give a lower value of d. In such a thin layer, two-dimensional effects should become important.

In the low-temperature range, the temperature dependence of magnetization arises from the excitation of the long-wavelength spin waves. Following the Heisenberg model, the temperature dependence of the hyperfine field can be written as

$$B_{hf}(T)/B_{hf}(0) = 1 - B(T/T_C)^{3/2} - C(T/T_C)^{5/2}. \tag{6}$$

Figure 9 gives the reduced hyperfine field of specimen A0 as a function of $(T/T_C)^{3/2}$. The solid curve represents the least-squares fit of the data in the temperature range $0.0 < T/T_C < 0.8$ with equation (6). The fitted values of B and C are 0.33 and 0.23, respectively. These values agree reasonably with those for the specimens with similar composition [16].

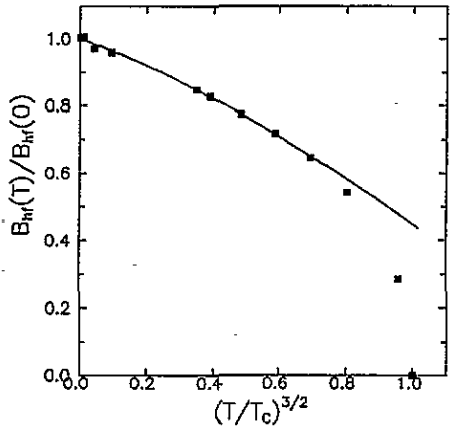

Figure 9. Reduced hyperfine field of specimen A0 as a function of $(T/T_C)^{3/2}$. The solid curve represents the fit to the data with equation (6).

The low-temperature hyperfine field data of specimen A2 also follow equation (6) with $B = 0.28$ and $C = 0.27$. For specimens A10 and A25, the low-temperature hyperfine field does not follow equation (6). Since the amount of nanocrystalline phase in these specimens is significantly large, a temperature-dependent interaction between the amorphous and nanocrystalline phases could be one possible reason for the deviation of the temperature dependence of low-temperature magnetization from equation (6).

Perusal of figure 6 shows that around 75 K the hyperfine field shows a steeper rise. If we take the dispersion relation for the spin waves as [17]

$$E(K) \simeq DK^2 \tag{7}$$

the wavelength of the spin waves at a temperature T may be written as

$$\lambda = 2\pi(D/k_BT)^{1/2}. \tag{8}$$

With decreasing temperature, the wavelength of the spin waves will increase. When the wavelength becomes comparable with the width of the grain boundary, the excitation of the spin waves will be hindered, causing a steeper increase in the hyperfine field. In some nanocrystalline specimens with composition very close to ours, the value of the spin-wave stiffness constant D is found to be 188 meV A^2 [16]. Using this value for D for our specimen, the temperature at which the wavelength of the spin wave becomes 42 Å is estimated as 50 K. Because the estimated value of 42 Å is the upper bound to the value of d, the agreement between the calculated and the experimentally observed temperature at which a steeper increase in B_{hf} is observed is reasonably good.

3.2. Magnetization behaviour of crystalline components

The size of nanocrystals in the present specimens is small enough to qualify them as single-domain particles [6]. Several interesting magnetic effects are associated with such a small particle size. In the case when the thermal energy k_BT is comparable with the magnetic anisotropy energy KV of a single-domain particle, the magnetic moment of the particle exhibits superparamagnetic relaxation and the hyperfine field collapses to zero. Even below the superparamagnetic blocking temperature, the hyperfine field may be reduced to a value below that for the bulk system because of the thermally excited fluctuations of the magnetization vector in directions close to an easy direction of magnetization (collective magnetic excitations).

For specimen A2, because of the small amount of the crystalline component, it was not possible to determine accurately the temperature dependence of different hyperfine field components. However, from figure 1(*b*) it is evident that the hyperfine field of the crystalline component decreases concurrently with that of the amorphous phase and collapses to zero around the Curie temperature of the amorphous phase. Thus, in this specimen the crystalline phase exhibits superparamagnetic relaxation, with its blocking temperature below the Curie temperature of the amorphous phase.

Figure 10 gives the dependence of the reduced hyperfine fields of the three main crystalline components of specimen A25 on the temperature. All the three components follow similar temperature dependences within experimental error. Therefore, in the following discussion, the analysis has been done taking the average of the three components.

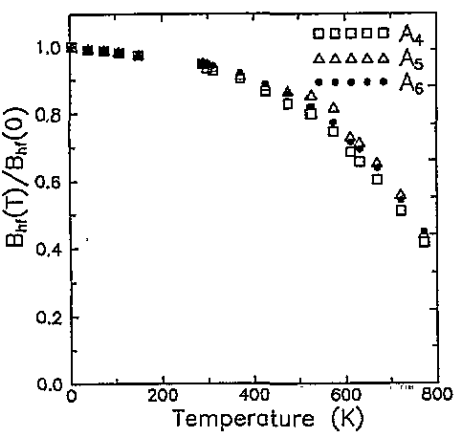

Figure 10. Reduced hyperfine fields of the three main crystalline components A_4, A_5 and A_6, for specimen A25 as a function of temperature.

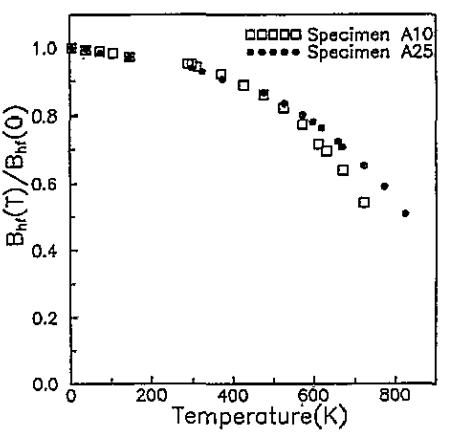

Figure 11. Variation in reduced average hyperfine field of the crystalline components for specimens A10 and A25 with temperature.

In the low-temperature region, the reduced hyperfine field was found not to follow equation (6). A fit of the data in the temperature range 4.2–150 K, of both specimen A10 and specimen A25 with a relation

$$B_{hf}(T)/B_{hf}(0) = 1 + bT^n \tag{9}$$

gave the value of the exponent n close to unity, indicating an almost linear temperature dependence in this range. In the high-temperature region, specimen A10 exhibits a faster decrease in $B_{hf}(T)$ compared with specimen A25 (figure 11) although from table 2 it is

evident that the compositions as well as the sizes of the nanocrystalline grains in the two specimens are the same. This peculiar behaviour of the magnetization may be understood in terms of the superferromagnetic interaction between the nanocrystalline grains. In the present system, since the thickness of the grain boundary layer is quite small, the magnetic dipole interaction between neighbouring grains would cause a ferromagnetic coupling between them, given by

$$E_{ij} = K_{\mathrm{m}}^{ij} M_i M_j \tag{10}$$

where K_{m}^{ij} is the magnetic coupling constant for the interaction between the crystallites i and j, and M_i is the magnetization of the ith crystallite. A modified mean field theory for such a system gives the temperature-dependent hyperfine field as [18, 19]

$$b(T) = \frac{B_{\mathrm{obs}}(T)}{B_0(T)} = L\left[\frac{3T_{\mathrm{p}}}{T}\left(\frac{B_0(T)}{B_0(T_{\mathrm{p}})}\right)^2 b(T)\right] \tag{11}$$

where $L[]$ is the Langevin function, $B_0(T)$ is the hyperfine field of the bulk and T_{p} is the magnetic transition temperature given by

$$T_{\mathrm{p}} = \frac{M^2(T_{\mathrm{p}})}{3k_{\mathrm{B}}} \sum_j K_{\mathrm{m}}^{ij}. \tag{12}$$

The temperature-dependent hyperfine field of the nanocrystalline phase at a temperature above the Curie temperature of amorphous phase, and in the presence of dipole interaction between the grains, will be given by equation (11). Since the compositions and the size of the nanocrystalline grains of specimens A10 and A25 are the same, the average magnetizations M_j of a grain are expected to be the same in the two specimens. However, since the degree of crystallization in the specimen A25 is higher, the average spacing between two nanocrystalline grains in this specimen will be smaller than that in specimen A10. This will lead to a higher value of K_{m}^{ij} and hence of T_{p} in specimen A25. Therefore, according to equation (11), the variation in hyperfine field with temperature for specimen A25 should be slower than for specimen A10. This agrees with the experimental data in figure 11. Thus, the observed temperature dependence of the hyperfine field of the crystalline component may be understood in terms of a superferromagnetic interaction between the nanocrystalline grains.

In the low-temperature range, equation (11) gives an almost linear temperature dependence of the hyperfine field [18]:

$$B_{\mathrm{obs}}(T) = B_0(T)\left[1 - \left(\frac{B_0(T_{\mathrm{p}})}{B_0(0)}\right)^2 \frac{T}{3T_{\mathrm{p}}}\right]. \tag{13}$$

In the present system, at low temperatures the amorphous phase is also in ferromagnetic state and will therefore contribute to the effective magnetic field at a nanocrystalline grain. However, this will not significantly modify the linear temperature dependence of the hyperfine field, as given by equation (13). Thus, the observed linear temperature dependence of the hyperfine field in the temperature range 4.2–140 K for specimens A10 and A25 provides further evidence for a superferromagnetic interaction between the nanocrystalline grains.

4. Conclusions

The main conclusions of the work can be summarized as follows.

In the as-prepared amorphous state, the magnetization behaviour of the specimen is similar to other transition-metal–metalloid metallic glasses with a broader distribution of exchange interaction and of magnetic moment. In the low-temperature region the temperature-dependent magnetization can be described in the terms of spin-wave excitation.

In partially crystallized specimens, the magnetization behaviours of both amorphous and nanocrystalline components are significantly different from those of bulk amorphous and crystalline Fe_3Si. In the critical region of the amorphous component, as the thickness of amorphous grain boundary decreases with increasing crystallization, the low-dimensional effects become evident. In the low-temperature range, the temperature dependence of the hyperfine field of amorphous component does not follow a $T^{3/2}$ behaviour. Around 75 K the hyperfine field of the amorphous phase exhibits a steeper rise due to damping of spin waves when the wavelength of the spin wave becomes comparable with the width of the amorphous grain boundary layer.

The size of the nanocrystalline grains qualifies it as a single-domain particle. Superparamagnetic relaxation is observed in the specimen annealed for 2 min. In the specimens annealed for longer times an increased number density of nanocrystalline grains cause a ferromagnetic interaction between them, modifying considerably the temperature dependence of their magnetization in both the low- and the high-temperature regions.

References

[1] Herzer G 1991 *Mater. Sci. Eng.* A **133** 1
[2] Yoshizawa Y 1988 *J. Appl. Phys.* **64** 6044
[3] Gupta A, Bhagat N and Principi G 1994 *J. Magn. Magn. Mater.* **133** 291
[4] Herzer G 1989 *IEEE Trans. Magn.* **25** 3327
[5] Kulik T and Hernando A 1992 *Proc. 1st Meet. on Magnetoelastic Effects and Applications* ed L Lanotte (Amsterdam: Elsevier) p87
[6] Chikazumi S 1966 *Physics of Magnetism* (New York: Wiley)
[7] Slawska-Wainewska A, Gutowski M, Lachowicz H K, Kulik T and Matyja H 1993 *Phys. Rev.* B
[8] Hample G, Pundt A and Hesse J 1992 *J. Phys.: Condens. Matter* 4 3195
[9] Stearns M B 1963 *Phys. Rev.* B **129** 1136
[10] Handrich K 1969 *Phys. Status Solidi* **32** K55
[11] Prasad B B, Bhatanagar A K and Jagannathan R 1980 *Solid State Commun.* **36** 661
[12] Kaneyoshi T and Tamura I 1984 *Phys. Status Solidi* b **123** 525
[13] Penissod P, Durand J and Budnick J I 1982 *Nucl. Instrum. Methods* **199** 99
[14] Bhatanagar A K, Prasad B B and Jagannathan R 1984 *Phys. Rev.* B 29 4896
Chien C L and Hasegawa R 1977 *Phys. Rev.* B **16** 3024
[15] Thomas M F and Johnson C E 1986 *Mössbauer Spectroscopy* ed D P E Dickson and F J Berry (Cambridge: Cambridge University Press) p 143
[16] Yu S, Kim K, Cho Y and Kim T 1992 *IEEE Trans. Magn.* **28** 5
[17] Moorjani K and Coey J M D 1984 *Magnetic Glasses* (Amsterdam: Elsevier) p 133
[18] Morup S 1983 *J. Magn. Magn. Mater.* **37** 39
[19] Morup S, Madsen M B, Franck J, Villadsen J and Koch C J W 1983 *J. Magn. Magn. Mater.* **40** 163